Multimodal image analysis and subvalvular dynamics in ischemic mitral regurgitation

Ahmed H. Aly, PhD,[a,b] Yoshiaki Saito, MD, PhD,[a,c] Wobbe Bouma, MD, PhD,[d] James J. Pilla, PhD,[a,e] Alison M. Pouch, PhD,[a,e] Paul A. Yushkevich, PhD,[e] Matthew J. Gillespie, MD,[a,f] Joseph H. Gorman III, MD,[a,g] and Robert C. Gorman, MD[a,g]

ABSTRACT

Background: The exact geometric pathogenesis of leaflet tethering in ischemic mitral regurgitation (IMR) and the relative contribution of each component of the mitral valve complex (MVC) remain largely unknown. In this study, we sought to further elucidate mitral valve (MV) leaflet remodeling and papillary muscle dynamics in an ovine model of IMR with magnetic resonance imaging (MRI) and 3-dimensional echocardiography (3DE).

Methods: Multimodal imaging combining 3DE and MRI was used to analyze the MVC at baseline, 30 minutes post–myocardial infarction (MI), and 12 weeks post-MI in ovine IMR models. Advanced 3D imaging software was used to trace the MVC from each modality, and the tracings were verified against resected specimens.

Results: 3DE MV remodeling was regionally heterogenous and observed primarily in the anterior leaflet, with significant increases in surface area, especially in A2 and A3. The posterior leaflet was significantly shortened in P2 and P3. Mean posteromedial papillary muscle (PMPM) volume was decreased from 1.9 ± 0.2 cm^3 at baseline to 0.9 ± 0.3 cm^3 at 12 weeks post-MI ($P < .05$). At 12 weeks post-MI, the PMPM was predominately displaced horizontally and outward along the intercommissural axis with minor apical displacement. The subvalvular contribution to tethering is a combination of unilateral movement, outward displacement, and degeneration of the PMPM. These findings have led to a proposed new framework for characterizing PMPM dynamics in IMR.

Conclusions: This study provides new insights into the complex interrelated and regionally heterogenous valvular and subvalvular mechanisms involved in the geometric pathogenesis of IMR tethering. (JTCVS Open 2021;5:48-60)

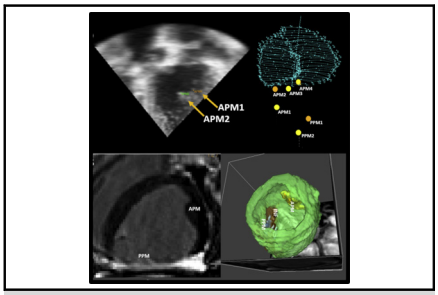

Multimodal imaging showing mitral valve leaflet remodeling is heterogenous and allows for papillary muscle staging.

CENTRAL MESSAGE

Multimodal imaging provides new insights into regionally heterogenous mitral valve leaflet remodeling and subvalvular mechanisms involved in the pathogenesis of ischemic mitral regurgitation tethering.

PERSPECTIVE

Noninvasive multimodal image analysis using magnetic resonance imaging for left ventricular and subvalvular assessment and 3-dimensional echocardiography for the mitral valve shows clinical promise and provides insight into the complex valvular and subvalvular interactions leading to ischemic mitral regurgitation (IMR). Given this clearer understanding, adjunct surgical repair strategies should aim to restore each component contributing to the geometric pathogenesis of IMR.

See Commentaries on pages 61 and 63.

From the [a]Gorman Cardiovascular Research Group, Perelman School of Medicine, University of Pennsylvania, Philadelphia, Pa; [b]Department of Bioengineering, University of Pennsylvania, Philadelphia, Pa; [c]Department of Thoracic and Cardiovascular Surgery, Hirosaki University, Aomori, Japan; [d]Department of Cardiothoracic Surgery, University of Groningen, University Medical Center Groningen, Groningen, The Netherlands; [e]Department of Radiology, Perelman School of Medicine, University of Pennsylvania, Philadelphia, Pa; [f]Department of Cardiology, The Children's Hospital of Philadelphia, Philadelphia, Pa; and [g]Department of Surgery, Perelman School of Medicine, University of Pennsylvania, Philadelphia, Pa.

Drs Aly and Saito contributed equally and are considered co–first authors.

This research was supported by grants from the National Heart, Lung, and Blood Institute of the National Institutes of Health (HL103723 and HL63954).

Received for publication Oct 9, 2020; accepted for publication Oct 9, 2020; available ahead of print Dec 5, 2020.

Address for reprints: Robert C. Gorman, MD, Gorman Cardiovascular Research Group, Smilow Center for Translational Research, 3400 Civic Center Blvd, Bldg 421, 11th Floor, Room 114, Philadelphia, PA, 19104-5156 (E-mail: robert.gorman@pennmedicine.upenn.edu).

2666-2736

https://doi.org/10.1016/j.xjon.2020.10.007

Abbreviations and Acronyms

2D = two-dimensional
3DE = 3-dimensional echocardiography
AC = anterior commissure
ALPM = anterolateral papillary muscle
ANC = annular center
BNM = bilateral noncongruent movement
IMR = ischemic mitral regurgitation
LV = left ventricular
MI = myocardial infarction
MV = mitral valve
MVC = mitral valve complex
PM = papillary muscle
PMPM = posteromedial papillary muscle

The main mechanism of ischemic mitral regurgitation (IMR) is a combination of annular dilatation and leaflet tethering caused by left ventricular (LV) remodeling and papillary muscle (PM) displacement after myocardial infarction (MI).[1] To develop successful adjunctive subvalvular repair mechanisms, the exact pathogenesis of tethering in IMR should be completely unraveled. IMR pathogenesis has long been studied in controlled IMR ovine models, owing to the difficulty in monitoring disease progression in patients. Invasive methods using sonomicrometry, tantalum, and radiopaque marker experiments have provided valuable insights[2-7]; however, their invasive nature makes them not clinically applicable. Meanwhile, noninvasive studies of subvalvular subunits of the mitral valve complex (MVC) have been limited primarily by the complexity of dynamic mitral geometry and the inherent limitations of available imaging modalities. This is especially true for the PMs, which are anatomically highly variable[8,9] and difficult to visualize with 3-dimensional echocardiography (3DE) owing to its low contrast. Compared with 3DE, magnetic resonance imaging (MRI) provides lower spatial and temporal resolution but higher contrast for improved visibility and more accurate volumetric measurements. Thus, 3DE is better suited for studying regional mitral valve (MV) geometry,[10,11] remodeling,[4] and MVC dynamics,[10,12] and MRI is more equipped for studying LV and papillary structural changes.[13] Image analysis of this synergistic combination of MRI and 3DE is likely to further our current understanding of the role of each component of the MVC and how it contributes to tethering pathogenesis.

In this study, we sought to elucidate geometric MV leaflet remodeling and PM dynamics in an ovine model of IMR with a multimodal imaging approach using MRI and 3DE. The study was designed to quantify dynamic geometric changes in the MVC in ovine IMR models at baseline (before MI), in the acute phase of IMR (30 minutes post-MI), and in the chronic phase of IMR (12 weeks post-MI) (Figure 1). We hypothesize that a multimodal image analysis approach using 3DE and MRI will comprehensively improve MV subunit analysis in IMR. To our knowledge, this is the first study to use a multimodal approach to analyze both valvular and subvalvular 3D geometric dynamic remodeling in an effort to unravel the exact pathogenesis of tethering in IMR.

METHODS

Surgical Protocol

Animals were treated under an experimental protocol in compliance with National Institutes of Health Guide for the Care and Use of Laboratory Animals (publication 85-23, revised 1996) and approved by the University of Pennsylvania's Institutional Animal Care and Use Committee. Healthy sheep (n = 6; mean weight, 50.2 ± 0.4 kg) were sedated, and a posterolateral infarction was induced by ligating the left circumflex artery distal to the first obtuse marginal branch, to target an infarction of approximately 20% of LV size. The post-MI animals were then monitored for several weeks, and terminal 3DE and MRI were performed at 12 weeks post-MI. A detailed description of the surgical protocol is provided in Appendix 1.

Echocardiographic Protocol

The 3DE images were acquired through direct epicardial echocardiography with a Phillips ie33 ultrasound system equipped with a 2- to 7- MHz X7-2t TEE matrix transducer (Philips Medical, Andover, Mass). MR severity was determined semiquantitatively with color Doppler by assessing the area of the regurgitant jet as a percentage of left atrial area in the apical 4-chamber view. MR was graded as 0, no MR; 1, <20%; 2, 20% to 40%; 3, 40% to 60%; and 4, >60%.[14]

3DE Image Segmentation

The 3DE data were exported to an Echo-View 5.4 software workstation (TomTec Imaging System, Munich, Germany). Both annular and leaflet tracings were acquired at mid-systole, and annular tracings were acquired at end-systole and end-diastole. Techniques of annular segmentation and modeling and leaflet segmentation and modeling have been described previously.[9,15-17] The various parameters measured are defined in Appendix 1.

MRI Image Acquisition and Reconstruction

MRIs were acquired using a 3-T clinical imaging system (Tim Trio Model, Siemens Healthcare, Erlangen, Germany) to generate cine and late gadolinium-enhanced cardiovascular imaging. Two-dimensional (2D) multislice images were reconstructed with volume segmentation and processing software (Seg3D; University of Utah Scientific Computing and Imaging Institute, Salt Lake City, Utah) (Figure 2). Volume data and muscle thickness were calculated with a resolution of 4.84 mm^3/pixel. A detailed description of the procedure is provided in Appendix 1.

Statistical Analysis

Continuous variables were expressed as mean ± SD, and the Shapiro–Wilk test for normality found all continuous variables to be normally distributed. Comparisons between each time point were performed with 1-way analysis of variance with Bonferroni correction. We used R (R Foundation for Statistical Computing, Vienna, Austria) and lme4[15] to perform a linear mixed-effects analysis of the relationship between time and leaflet measurements. As the fixed effect, we entered time points and as the random effect we had intercepts for subjects in the model and reported the fixed-effect correlations. MRI data were obtained at baseline and 12 weeks post-MI, and comparisons between time points were made using the paired-samples *t* test. All calculations were performed with SPSS 21.0

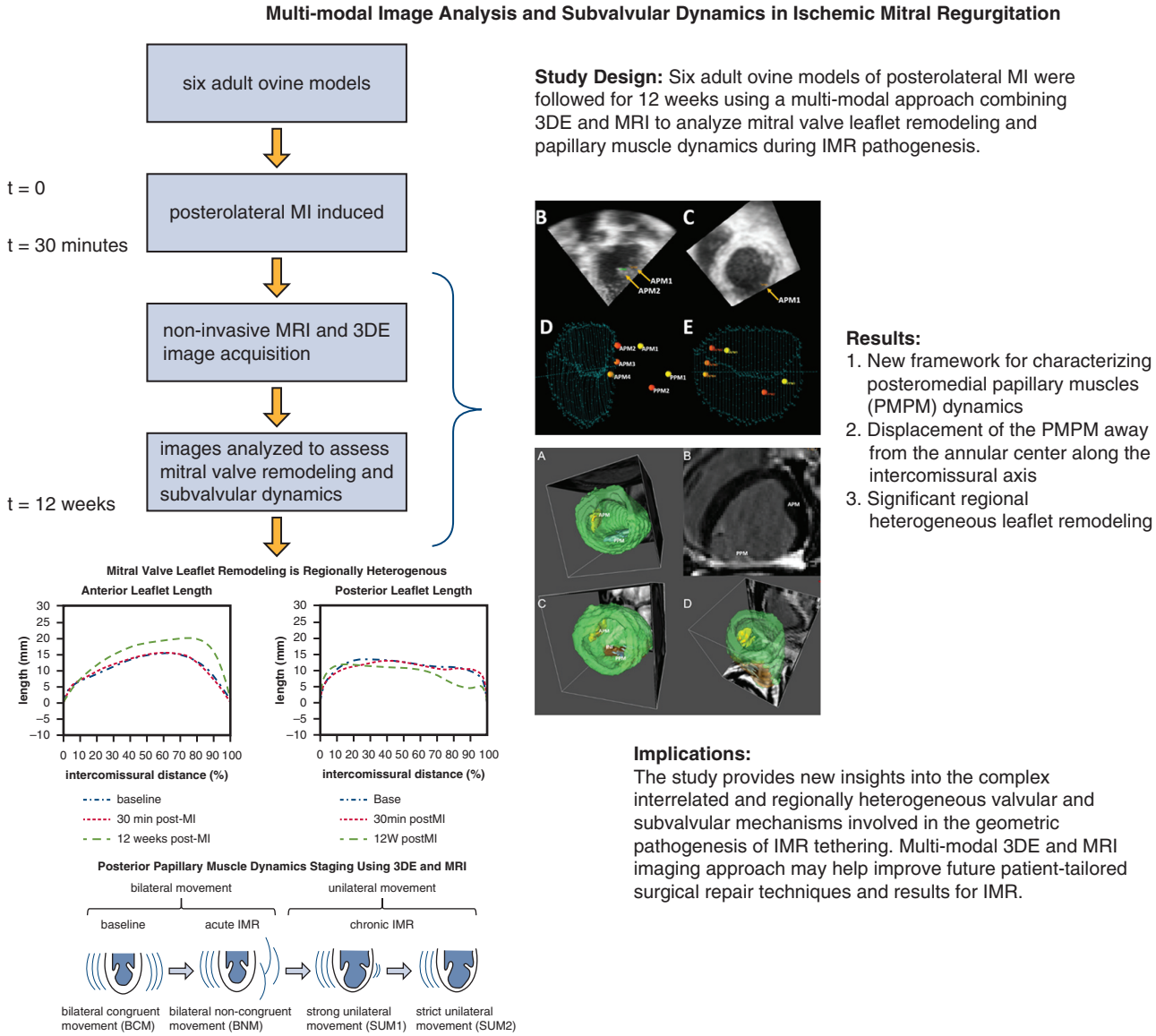

FIGURE 1. Overview of the study. Using magnetic resonance imaging and 3-dimensional echocardiography, we followed 6 ischemic mitral regurgitation (*IMR*) ovine models at baseline, 30 minutes post–myocardial infarction (*MI*), and 12 weeks post-MI to study the valvular and subvalvular apparatus of the mitral valve in IMR. This could allow for better preoperative planning and tailoring of adjunct surgical treatment.

(IBM, Armonk, NY). Statistically significant differences were established at $P < .05$.

RESULTS

MRI Subvalvular Volumetric Data

Total ventricular muscle volume did not change significantly over 12 weeks, and the infarcted muscle volume ratio was 9.4 ± 1.3% at 12 weeks post-MI. Although anterolateral PM (ALPM) volume remained relatively constant, mean posteromedial PM (PMPM) volume decreased significantly, from 1.9 ± 0.2 cm^3 at baseline to 0.9 ± 0.3 cm^3 at 12 weeks post-MI ($P < .05$). Posterior LV wall thickness decreased significantly, from 9.0 ± 0.6 mm to 4.8 ± 0.5 mm ($P < .05$), whereas anterior and septal wall thickness did not change. LV end-diastolic volume increased from 86.4 ± 13.0 mL to 128.7 ± 23.0 mL ($P < .05$) due to LV dilation after ischemia. LV ejection fraction decreased from 61.1 ± 5.9% at baseline to 42.8 ± 5.5% at 12 weeks post-MI ($P < .001$) (Table 1).

3D Mitral Leaflet Remodeling Data

Total mitral leaflet area was expanded from 730 ± 84 mm^2 at baseline to 849 ± 67 mm^2 at 12 weeks post-MI ($P = .07$). Interestingly, leaflet area expansion was dominated by anterior leaflet enlargement from 363 ± 85 mm^2 at baseline to 526 ± 67 mm^2 at 12 weeks

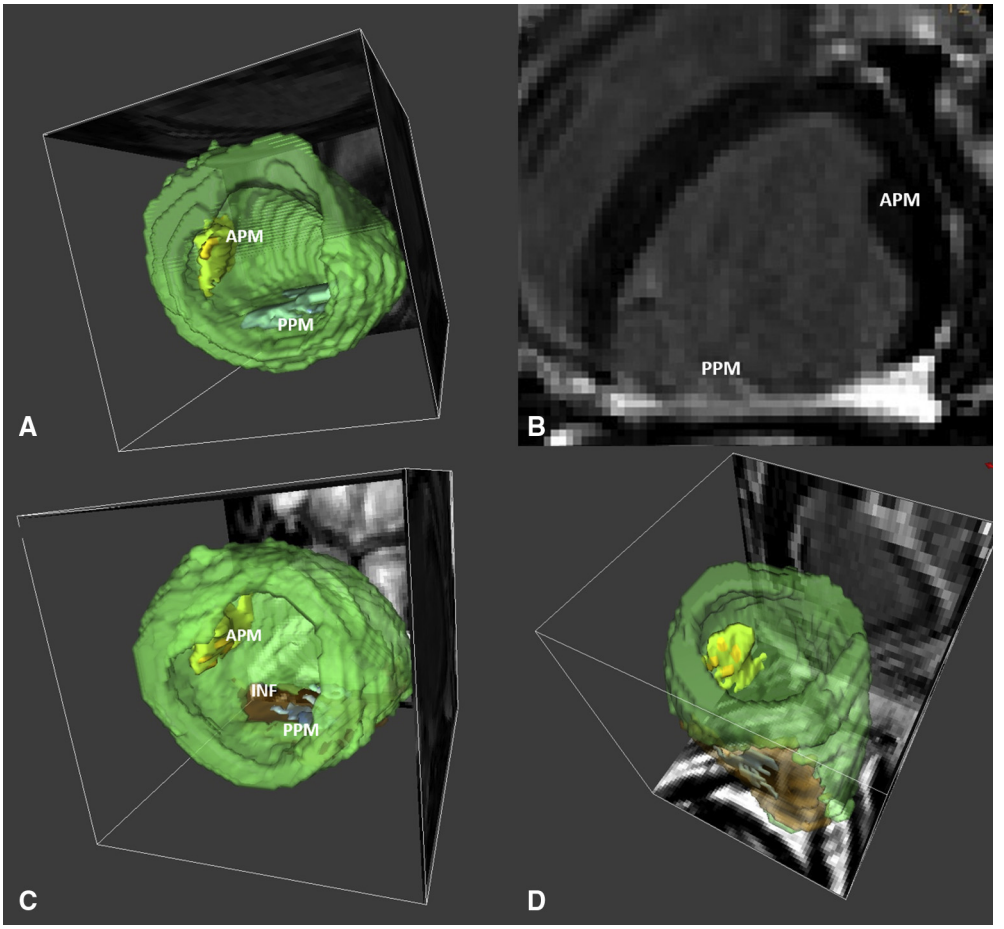

FIGURE 2. Magnetic resonance imaging (MRI) image processing technique. Two-dimensional multislice images were reconstructed with volume segmentation and processing software. A, Reconstructed 3-dimensional (3D) model of baseline MRI. The anterolateral papillary muscle (*ALPM*) is marked with *yellow*, and the posteromedial papillary muscle (*PMPM*) is in *light blue*. B, Late gadolinium-enhanced MRI at 12 weeks after myocardial infarction (MI). Short-axis view. C and D, 3D reconstructed model at 12 weeks post-MI in the same animal as in A. The infarcted area (*INF*) is marked in brown. C, Atrial view. D, Posteromedial view.

post-MI ($P < .001$). In contrast, posterior leaflet area decreased at 12 weeks post-MI compared with baseline. Furthermore, average regional leaflet lengths demonstrated significant anterior leaflet elongation in all segments, especially in A2 and A3, which corresponded to significant P2 and P3 shortening relative to baseline at 12 weeks post-MI. Figure 3 shows the progression of average leaflet elongation along the intercommissural axis across all subjects

TABLE 1. MRI volumetric data

Variable	Baseline	12 wk post-MI
LV muscle volume (infarcted muscle volume), cm^3	99.5 ± 12.3	102.6 ± 16.3 (10.0 ± 4.2)
Anterolateral papillary muscle volume, cm^3	2.7 ± 1.1	3.3 ± 1.2*
Posteromedial papillary muscle volume, cm^3	1.9 ± 0.2	0.9 ± 0.3*
Anterior ventricular wall thickness, mm	8.1 ± 0.3	8.8 ± 0.9
Posterior ventricular wall thickness, mm	9.0 ± 0.6	4.8 ± 0.5*
Septal ventricular wall thickness, mm	9.5 ± 0.5	10.1 ± 0.9
LVEF, %	61.1 ± 5.9	42.8 ± 5.5*
LVEDV, mL	86.4 ± 13.0	128.7 ± 23.0*
LVESV, mL	33.8 ± 8.2	74.2 ± 19.5*

All values are mean ± SD. *MI*, Myocardial infarction; *LV*, left ventricular; *LVEF*, left ventricular ejection fraction; *LVEDV*, left ventricular end-diastolic volume; *LVESV*, left ventricular end-systolic volume. *$P < .05$ vs baseline.

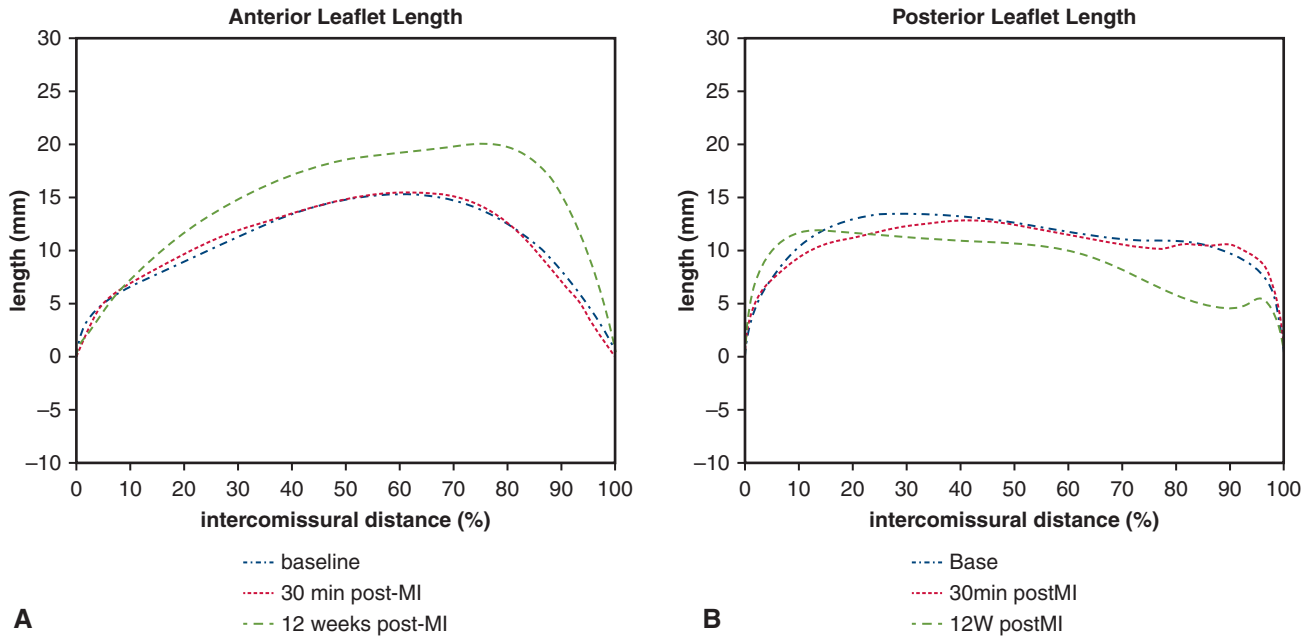

FIGURE 3. Regional mitral valve (MV) leaflet adaptation. A, Regional anterior MV leaflet length at baseline (*blue*), 30 minutes post–myocardial infarction (*MI*) (*red*), and 12 weeks post-MI (*green*). The leaflet length is plotted as a function of intercommissural distance, expressed as a percentage of the distance traveled from the anterior commissure (AC). The positions of the AC and posterior commissure (PC) are 0% and 100%, respectively. B, Regional posterior valve leaflet length at baseline (*blue*), 30 minutes post-MI (*red*), and 12 weeks post-MI (*green*).

for each leaflet, highlighting the anterior leaflet elongation in the A2 and A3 regions and posterior leaflet shortening in the P2 and P3 regions. Table 2 summarizes the average leaflet lengths for each anatomic MV valve scallop.

Papillary Muscle Orientation and Dynamics

The 3DE annular and PM tip landmarks showed PMPM displacement with significantly increased distance between the PMPM tip to the annular center (ANC) in the diastolic phase from 22.7 ± 3.3 mm at baseline to 30.3 ± 3.4 mm at 12 weeks post-MI ($P < .05$) (Table 3). This significant PMPM to ANC distance increase was not present at 30 minutes post-MI. In contrast, the ALPM to ANC distance remained constant. At 12 weeks post-MI, mean interpapillary muscle distance increased from 30.1 ± 1.9 mm in diastole and 20.6 ± 2.9 mm in systole, to 37.2 ± 5.9 mm in diastole ($P < .05$), and to 33.3 ± 5.0 mm in systole ($P < .05$).

To study PM dynamics and position, the ANC was aligned throughout each contraction and used as the origin of the coordinate system shown in Figure 4. At baseline, ALPM and PMPM tip positions changed throughout the cardiac cycle. ALPM and PMPM moved toward the center of the annulus and toward the ventricular apex away from the positive Z direction in the systolic phase. Compared with the diastolic phase, the ALPM to ANC and PMPM to ANC distances decreased during systole by an average of 1.8 mm and 1.7 mm, respectively. At 30 minutes post-MI, PMPM movement was constrained throughout the

TABLE 2. Mitral valve regional leaflet remodeling

Variable	Baseline	30 min post-MI	12 wk post-MI	Fixed-effect correlation
Leaflet length, mm				
A1	8.1 ± 2.0	8.4 ± 1.5	10.3 ± 1.1*,†	0.690
A2 (left half)	13.6 ± 1.4	13.7 ± 1.8	17.4 ± 0.5*,†	0.879
A2 (right half)	15.2 ± 1.4	15.3 ± 1.4	19.2 ± 0.8*,†	0.877
A3	10.6 ± 1.9	10.8 ± 0.6	16.5 ± 2.3*,†	0.926
P1	11.0 ± 2.6	10.0 ± 1.6	10.8 ± 2.2	0.592
P2 (left half)	13.1 ± 3.0	12.7 ± 2.6	11.0 ± 2.9*	0.549
P2 (right half)	12.0 ± 3.0	11.6 ± 1.9	10.1 ± 2.8*	0.570
P3	9.8 ± 3.1	9.8 ± 2.9	5.9 ± 1.3*,†	0.831

All values are mean ± SD. *MI*, Myocardial infarction. *$P < .05$ vs baseline. †$P < .05$ vs 30 min post-MI.

TABLE 3. End-diastolic and end-systolic interpapillary muscle distance and papillary muscle to annular distance

Parameter	Baseline		30 min post-MI		12 wk post-MI	
	ED	ES	ED	ES	ED	ES
ALPM to, mm						
mid-AA	26.9 ± 3.0	26.6 ± 2.9	28.1 ± 1.8	28.8 ± 2.3	28.9 ± 2.1	30.1 ± 3.5*
AC	19.4 ± 3.4	19.7 ± 2.2	19.6 ± 2.9	20.8 ± 2.5	22.0 ± 4.1	20.4 ± 4.0
PC	36.1 ± 2.5	30.3 ± 2.6	36.9 ± 1.1	33.0 ± 2.2	38.4 ± 2.5†	34.4 ± 3.9*
mid-PA	29.0 ± 3.3	28.1 ± 2.2	29.5 ± 2.7	27.9 ± 2.5	28.4 ± 3.6	27.3 ± 5.3
ANC	24.2 ± 2.2	22.4 ± 1.7	24.9 ± 1.8	23.7 ± 2.0	23.8 ± 1.8	24.1 ± 3.2
PMPM to, mm						
mid-AA	29.3 ± 3.2	28.8 ± 2.7	29.2 ± 0.8	30.7 ± 1.4	37.0 ± 3.1†‡	38.1 ± 4.1*§
AC	34.4 ± 5.3	30.4 ± 5.3	35.5 ± 2.4	31.3 ± 2.7	46.0 ± 3.8†‡	42.3 ± 4.1*§
PC	20.3 ± 2.8	19.4 ± 2.5	21.0 ± 2.6	21.5 ± 1.3	25.7 ± 2.3†‡	24.6 ± 1.6*§
mid-PA	23.5 ± 4.0	23.0 ± 2.5	23.4 ± 1.6	21.2 ± 2.6	30.0 ± 4.7†‡	28.5 ± 3.9*§
ANC	22.7 ± 3.3	21.0 ± 2.9	22.4 ± 1.7	21.2 ± 1.3	30.3 ± 3.4†‡	29.8 ± 3.5*§
ALPM - PMPM distance, mm	30.1 ± 1.9	20.6 ± 2.9	29.8 ± 2.6	22.7 ± 3.8	37.2 ± 5.9†‡	33.3 ± 5.0*§

All values are mean ± SD. *MI*, Myocardial infarction; *ED*, end-diastolic phase; *ES*, end-systolic phase; *ALPM*, anterolateral papillary muscle; *AA*, anterior mitral annulus; *AC*, anterior commissure; *PC*, posterior commissure; *PA*, posterior mitral annulus; *ANC*, mitral annular center; *PMPM*, posteromedial papillary muscle. *$P < .05$ vs baseline end-systolic phase. †$P < .05$ vs baseline end-diastolic phase. ‡$P < .05$ vs 30 min post-MI end-diastolic phase. §$P < .05$ vs 30 min post-MI end-systolic phase.

contraction cycle, but the PMPM to ANC distance remained the same as baseline. At 12 weeks post-MI, the PMPM was static throughout the cycle, whereas ALPM movement was preserved. Figure 5 shows the geometric relationship between annulus and PM positions throughout contraction cycles across all time points and animals.

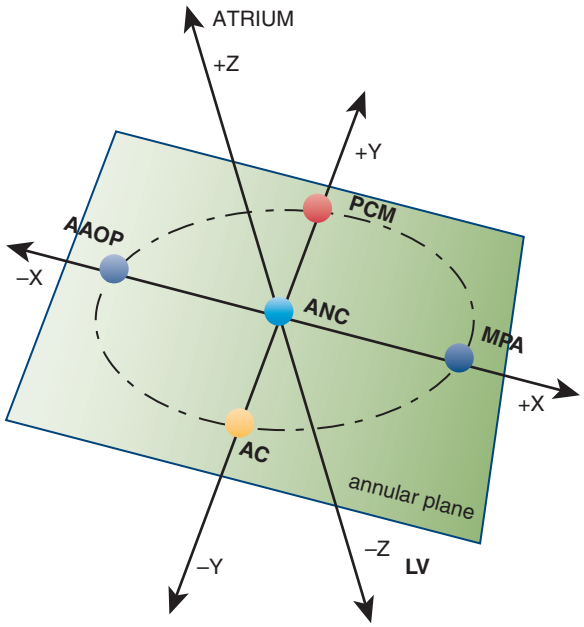

FIGURE 4. Coordinate system used to calculate position and dynamics of the papillary muscles. The mitral annular center (*ANC*) was set as the coordinate origin. We defined the positive *X* direction as the vector pointing toward the posterior horn of the mitral annulus. We defined the positive *Y* direction as the vector pointing toward the posterior commissure and the positive *Z* direction as the vector pointing toward the left atrial roof. *PCM*, Posterior commissure; *AAOP*, anterior aortic peak; *MPA*, midpoint of posterior annulus; *AC*, anterior commissure; *LV*, left ventricular.

DISCUSSION

In this study, we analyzed MV leaflet remodeling and PM structure and dynamics in IMR pathogenesis using both noninvasive MRI and 3DE. To our knowledge, this is the first study to combine 3DE and MRI to comprehensively assess both valvular and subvalvular components of the MVC during IMR pathogenesis. The key findings of this study are (1) a new framework for characterizing PMPM dynamics, (2) displacement of the PMPM away from the ANC along the intercomissural axis, and (3) significant regionally heterogeneous leaflet remodeling.

From 3DE and MRI, we characterize PM dynamics more definitely with a new framework summarized in Figure 6. At baseline, the PM display bilateral congruent movement, with the PM moving along the intercomissural axis and slightly toward the apex, preserving the distance between the PM and ANC. Bilateral noncongruent movement (BNM) was observed after acute MI. In BNM, PMPM movement is dampened along the intercomissural axis relative to baseline with preserved PMPM to ANC distance. Despite BNM, the development of MR was not significantly different between baseline and after acute MI. At 12 weeks post-MI, PM dynamics demonstrated strong unilateral movement with minimal PMPM motion and strict unilateral movement with a completely immobile PMPM. In contrast to acute-phase MI, moderate to severe MR developed in all the animals. Compared with that at baseline and acute post-MI, the systolic PMPM to ANC distance was larger by an average as 8.8 mm and 8.6 mm, respectively. At 12 weeks post-MI, the PMPM was displaced outward along the intercomissural axis, and the PMPM volume was significantly

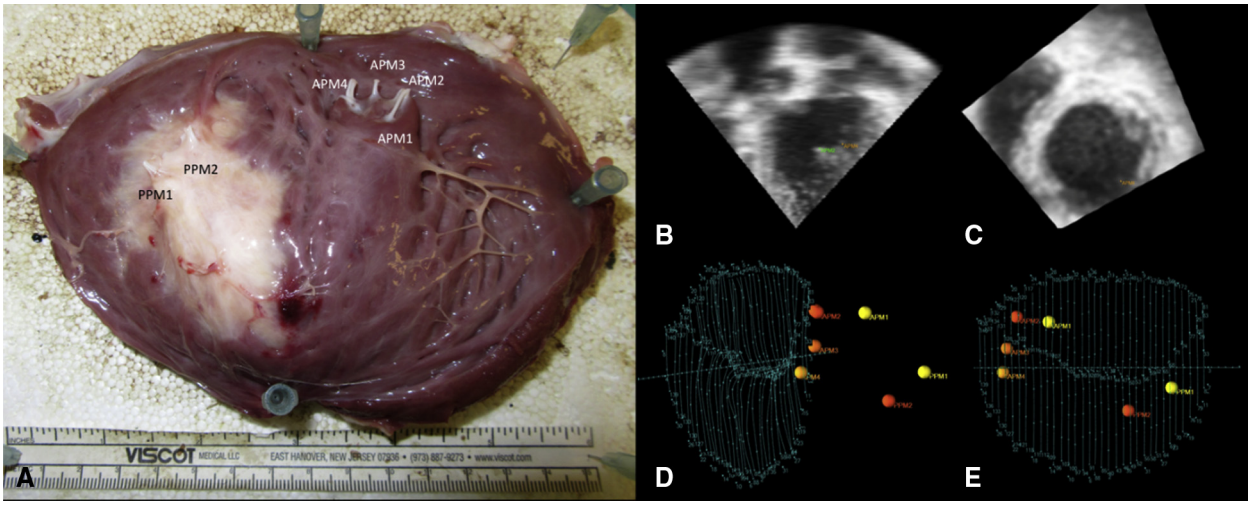

FIGURE 5. Papillary muscle (PM) tracing technique. A, Resected heart after euthanization. The right ventricle and atria were removed, and the left ventricular septum was cut longitudinally from the aortic root toward the apex. The number of PM tips and anatomic characteristics were identified. B, Oblique view of 2-dimensional echocardiography (2DE) at baseline. PM tips were marked according to the anatomic characteristics obtained from the resected specimen. C, Short-axis view of 2-DE with the PMs marked. D and E, Traced annulus and leaflets along with marked PMs in right lateral oblique view (D) and front view from the left atrial side (E). *ALPM*, Anterolateral papillary muscle; *PMPM*, posteromedial papillary muscle.

decreased. The staging of PM dynamics and structure in IMR allows for more defined characterization of IMR and could allow for more carefully patient-tailored treatments.

Recent clinical imaging studies have shown that PM structure and dynamics contribute to IMR pathogenesis.[13,16,17] Our observation of strong unilateral movement at 12 weeks post-MI confirm what Padala and colleagues[13] found in a cohort of 67 patients using MRI. In their study, they demonstrated that MR is caused by the lack of shortening of interpapillary muscle distance from diastole to systole. In our study, we measured both the interpapillary muscle distance and the PM to ANC distance to capture both the displacement between the PMs and "dynamic congruence," which describe the magnitude and synchronization of PM motion. We found that the PM to ANC distance increased as IMR progressed. Thus, the subvalvular contribution to tethering may be a combination of strong/strict unilateral movement, outward displacement, and degeneration of the PMPM.

From 3DE-derived manual tracings of the mitral leaflets, we demonstrated the first instance of regionally heterogeneous leaflet remodeling in IMR. Our results in an ovine model show a significant increase in mean anterior leaflet surface area from 363 $\pm$ 85 mm^2 to 526 $\pm$ 67 mm^2 from baseline to 12 weeks post-MI. This increase in leaflet area mimics leaflet remodeling in humans. In contrast, the mean posterior leaflet area was decreased from

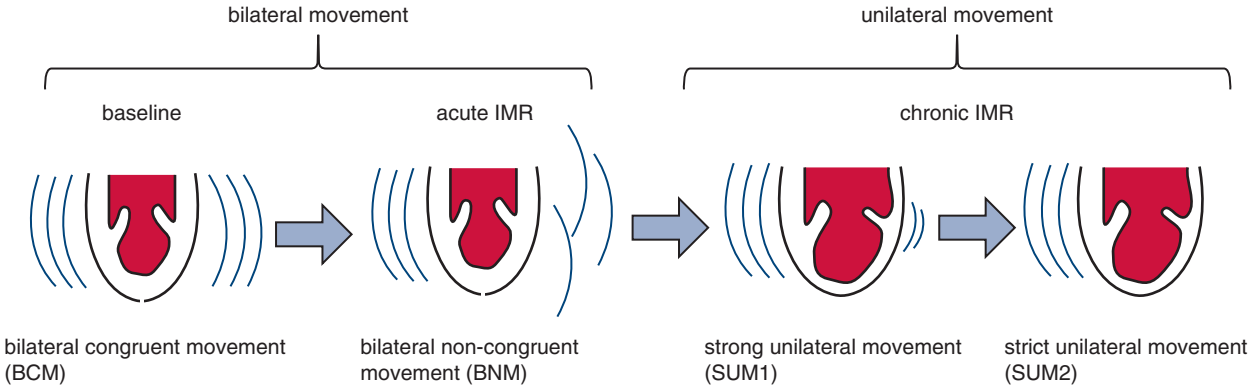

FIGURE 6. A new papillary dynamics framework in ischemic mitral regurgitation (*IMR*) pathogenesis. At baseline, papillary muscle (PM) movement can be described as bilateral congruent movement with full range of motion and preserved PM to the annular center distance (PM-ANC). In the acute phase of IMR, the PPM motion is dampened with preserved PM-ANC and can thus be described as bilateral noncongruent movement. In chronic IMR, the PM movement is unilateral with minimal PPM movement (SUM1) or strictly no PPM movement (SUM2). *SUM*, Strict unilateral movement.

TABLE 4. 3DE-derived measurements and landmarks

Landmarks and measurements	Definition
Anterior and posterior commissures	Annular points at the junction between the anterior and posterior leaflets
Annular height, mm	Distance between the midpoint of the anterior annulus and the best-fitted plane to annulus
Intercommissural width, mm	Distance between the commissures
Septolateral diameter, mm	Distance between the anterior and posterior annular midpoints
Annular height to commissural width ratio	Metric of global annular nonplanarity
Annular area, mm^2	Area of the annular projection onto the least-squares plane
Tenting area, mm^2	Area enclosed between the mitral leaflets and the annular plane
Tenting index, mm	Tenting volume divided by the mitral annular area
Anterior and posterior tenting angles, °	Angle formed by the line tangent to the anterior or posterior leaflet and the mitral annular plane computed
Mean segmental tethering angles, °	Mean tethering angles for the 6 leaflet regions A1, A2, A3, P1, P2, and P3
Coaptation area, mm^2	Sum of the incremental coaptation length along the intercommissural axis
Total leaflet area, mm^2	Sum of the incremental leaflet lengths
Anterolateral papillary muscle tip	Landmark at chordae endpoints attached in the region between A1, A2 and P1, P2*
Posteromedial papillary muscle tip	Landmark at chordae endpoints attached in the regions A2, A3 and P2, P3*

*The papillary muscle tips were traced retrospectively using resected heart specimens as ground truth for tracing the papillary muscle tips with the TOMTEC. If several papillary muscle tips were identified in 3D images, the coordinates were averaged.

367 ± 119 mm^2 at baseline to 324 ± 98 mm^2 at 12 weeks post-MI, with the average P2 and P3 leaflet lengths showing significant decreases. Anterior leaflet elongation and posterior leaflet shortening are plotted as a function of distance along the intercommissural axis in Figure 3.

In the context of recent experimental studies, our findings offer new insights into mitral leaflet remodeling—specifically, the regionally heterogenous leaflet response. Mitral leaflet remodeling was first described in animal models by Chaput and colleagues[18] as the increase in mitral leaflet area to reduce the severity of functional MR exacerbated by leaflet tethering due to LV remodeling. These findings were later confirmed clinically by Nishino and colleagues,[19] who reported increased total leaflet surface area in patients with chronic IMR compared with those with acute IMR. Subsequent animal experiments aimed at elucidating the cause of MV elongation in ischemic cardiomyopathy and have shown leaflet response changes in the setting of MI even if remodeling is prevented.[4,20] These experiments imply that infarction alone without LV remodeling may cause changes in the biological milieu leading to the hypothesized reactivation of the embryonic pathways that cause leaflet growth.

In a complementary experiment, Rausch and colleagues[21] demonstrated the effects of chronic mechanical strain caused by tethering and annular dilatation and showed chronic radial and circumferential growth in leaflets without significant regional variations, despite the variations in strain.[21] However, it is important to note that these insightful experiments analyzed the unloaded MV at 6 weeks[21] and 8 weeks[4] post-MI, limiting the time frame of chronic IMR analyzed. To address this limitation, we used 3DE to analyze the MV in mid-systole after 12 weeks post-MI. In the context of these recent experiments, our results suggest that regional variations in leaflet remodeling may be influenced by the variations in mechanical response reported by Rausch and colleagues and may be a result of leaflet stretching rather than biological growth.[21]

TABLE 5. Hemodynamic parameters and degree of mitral regurgitation

Hemodynamic parameter	Baseline	30 min post-MI	12 wk post-MI
Heart rate, bpm	89.5 ± 14.0	88.5 ± 5.1	96.7 ± 15.0
Systolic ABP, mm Hg	105.7 ± 14.9	96.3 ± 8.6	103.0 ± 13.5
Systolic PAP, mm Hg	25.7 ± 5.2	33.0 ± 7.1*	35.3 ± 3.8*
PCWP, mm Hg	12.0 ± 1.8	17.3 ± 5.0*	19.7 ± 1.9*,†
CVP, mm Hg	6.6 ± 1.8	9.0 ± 4.5	8.3 ± 3.1
Degree of MR	0.7 ± 0.5	1.0 ± 0.6	3.2 ± 0.4*,†

All values are shown in mean ± SD. *MI*, Myocardial infarction; *ABP*, arterial blood pressure; *PAP*, pulmonary arterial pressure; *PCWP*, pulmonary capillary wedge pressure; *CVP*, central venous pressure; *MR*, mitral regurgitation. *$P < .05$ vs baseline. †$P < .05$ vs 30 min post-MI.

Clinical Insights

From these findings, we glean clinical insights by distilling the mixture of mechanisms categorically into annular dilatation, papillary displacement and atrophy, and limited leaflet remodeling. Given this clearer

TABLE 6. Mitral valve geometric data in the systolic phase

Variable	Baseline	30-min post-MI	12 wk post-MI	Fixed-effect correlation
Mitral annular area, mm^2	682 ± 133	703 ± 105	822 ± 192*	0.641
Septolateral diameter, mm	25.9 ± 2.5	27.0 ± 2.1	28.8 ± 3.1*	0.594
Commissural width, mm^2	33.2 ± 3.8	32.8 ± 2.7	36.3 ± 4.2*,†	0.665
Transverse diameter, mm	32.7 ± 3.4	33.1 ± 2.9	36.5 ± 3.8*,†	0.682
Annular circumference, mm	101 ± 10	102 ± 8	113 ± 12*,†	0.697
Annular height, mm	4.0 ± 1.5	3.7 ± 0.9	3.8 ± 0.9	
Annular height:commissural width ratio, %	11.8 ± 3.9	10.7 ± 2.5	10.2 ± 3.0	
Mitral valve leaflet area, mm^2	730 ± 84	715 ± 90	849 ± 67	0.732
Anterior leaflet	363 ± 85	366 ± 52	526 ± 67*,†	0.837
Posterior leaflet	367 ± 119	349 ± 80	324 ± 98	0.623
Mitral valve tenting volume, mm^3	456 ± 206	657 ± 448	1496 ± 629*,†	0.888
Mitral valve tenting index	0.71 ± 0.45	0.94 ± 0.63	1.77 ± 0.52*	0.816
Segmental tethering angle, °				
A1	6.1 ± 3.4	8.4 ± 3.4	11.4 ± 3.2*	0.823
A2	8.7 ± 5.8	10.4 ± 6.4	14.5 ± 4.6*	0.711
A3	3.2 ± 2.2	3.7 ± 2.8	5.9 ± 1.9*	0.740
P1	4.9 ± 3.2	7.1 ± 3.2	10.3 ± 1.6*	0.846
P2	10.4 ± 7.5	12.3 ± 6.6	27.3 ± 8.7*,†	0.742
P3	3.3 ± 2.4	3.8 ± 2.4	20.0 ± 9.0*,†	0.916

All values are mean ± SD. *MI*, Myocardial infarction. *$P < .05$ vs baseline. †$P < .05$ vs 30 minutes post-MI.

understanding, adjunct surgical repair strategies should aim to restore each component. For this discussion, we focus on adjunct repair strategies in the context of the novel findings in our study. Based on the finding in this study, PM suspension should reposition the PMPM inward along the intercommissural axis to restore subvalvular geometry. This is contrary to current techniques that suspend the PMPM toward the posterior annulus or plicate the PMs. An alternative method is anterior repositioning of the PMPM, which has proven successful when combined with ring annuloplasty repair, with a 96% remission of grade 3+ MR at 2 years after repair.[22] A 2016 study also demonstrated that PM approximation significantly reduced recurrence of moderate-to-severe MR after surgery.[23] Second, midsystolic P2 and P3 shortening can be addressed with posterior leaflet augmentation.[24,25] Further studies are needed to prove effectiveness and long-term durability for these repair strategies. In terms of clinical prospect, noninvasive multimodal image analysis using MRI for LV and subvalvular assessment and 3DE for the MV shows clinical promise. With the increased availability of fast automated algorithms,[26,27] the automatic fusion and analysis of both modalities may be possible.[28]

TABLE 7. LV parameters from resected specimens 12 weeks after MI

Parameter	12 wk post-MI
LV weight, g	214.4 ± 29.0
LV area, cm^2	112.0 ± 17.6
LV infarction area, cm^2	25.2 ± 5.3
LV infarction ratio, %	22.4 ± 1.4
Number of ALPM heads	2.8 ± 0.8
Number of PMPM heads	2.2 ± 0.4

Values are mean ± SD. *MI*, Myocardial infarction; *LV*, left ventricular; *ALPM*, anterolateral papillary muscle; *PMPM*, posteromedial papillary muscle.

Limitations

The results of this study should be interpreted with some considerations. The primary strength of this study is the use of complimentary imaging modalities, 3DE and MRI, to analyze the valvular and subvalvular components of the MVC in IMR. A potential limitation is that the MRI and 3DE images were not acquired from the same cardiac cycle. However, we ensured that there were no circulatory instabilities throughout the imaging procedures to avoid inaccuracies. Other limitations are related to IMR quantification. Alternative methods for IMR severity assessment, such as regurgitant volume and effective regurgitant orifice area, were not available in this study. Jet area divided by LA area IMR quantification was used to confirm that sufficient

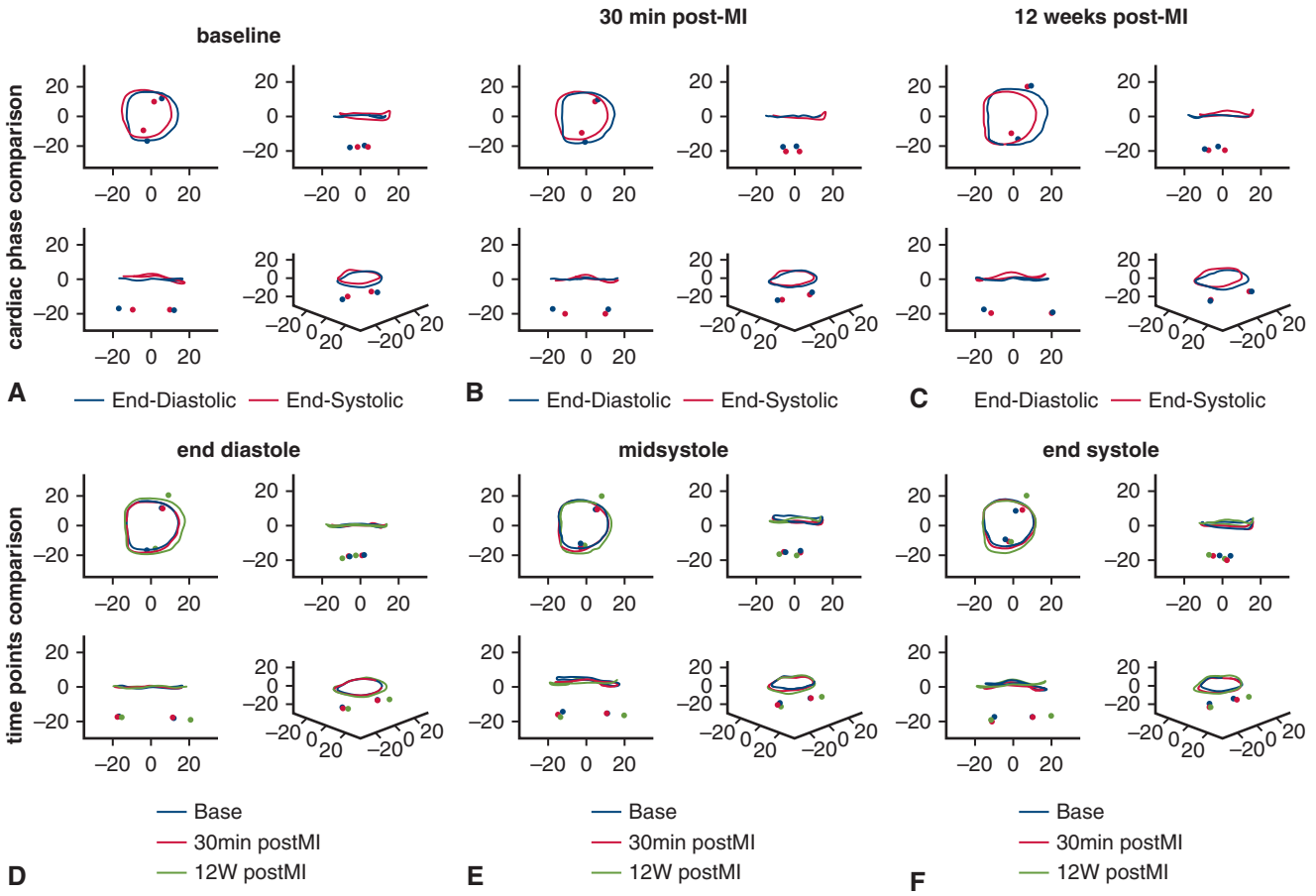

FIGURE 7. Temporal papillary muscle (PM) and annular dynamics throughout the cardiac cycle at serial time points. The *top row* compares mean annular and PM positions at end-diastole (*blue*) and at end-systole (*red*) in the atrial plane (*left upper corner*), Septolateral plane (*right upper corner*), intercomissural plane (*left lower corner*), and 3-dimensional view (*right lower corner*) at A, baseline; B, 30 minutes post–myocardial infarction (*MI*); and C, 12 weeks post-MI. The annuli are represented by *circular shapes*, and the PMs are represented by *dots*. The annular center was set as the origin. A, anterior annulus; L, left lateral annulus; P, posterior annulus; R, right lateral portion of the mitral annulus. The *bottom row* shows comparisons between mean annular and PM positions at baseline (base; *blue*), 30 minutes post-MI (*red*), and 12 weeks post-MI (*green*) at 3 different cardiac phases: D, end-diastole; E, mid-systole; F, end-systole. Table 8 shows the geometric papillary muscle position in Cartesian coordinates throughout cardiac cycle.

TABLE 8. Geometric papillary muscle position in Cartesian coordinates throughout cardiac cycle

	Baseline			30 min post-MI			12 wk post-MI		
Coordinates	**ED**	**ES**	**ES-ED**	**ED**	**ES**	**ES-ED**	**ED**	**ES**	**ES-ED**
ALPM									
position, mm									
X	−2.1 ± 2.7	−1.7 ± 2.6	0.3 ± 2.3	−0.7 ± 2.7	−1.0 ± 2.0	−0.3 ± 1.9	2.4 ± 2.4	1.2 ± 3.3	1.2 ± 1.9
Y	−16.7 ± 2.7	−11.5 ± 3.9	5.2 ± 1.5	−17.4 ± 2.4	−11.8 ± 3.2	5.6 ± 1.2	−15.4 ± 3.4	−10.6 ± 4.5	4.8 ± 2.7
Z	−17.0 ± 2.9	−18.6 ± 2.0	−1.6 ± 2.7	−17.5 ± 2.1	−20.3 ± 1.9	−2.8 ± 1.3	−17.5 ± 3.0	−21.0 ± 3.8	−3.5 ± 3.3
PMPM									
position, mm									
X	5.6 ± 1.8	3.8 ± 2.4	1.8 ± 1.4	6.2 ± 1.2	6.0 ± 2.6	0.2 ± 2.0	9.3 ± 5.0	9.5 ± 3.9	−0.2 ± 1.7
Y	12.0 ± 4.2	8.0 ± 4.2	3.9 ± 2.1	11.4 ± 3.8	9.3 ± 3.4	2.1 ± 1.9	20.7 ± 4.6	20.8 ± 3.9	−0.1 ± 2.6
Z	−18.1 ± 2.7	−18.6 ± 2.2	−0.5 ± 1.8	−17.8 ± 2.7	−17.6 ± 1.8	0.2 ± 2.7	−19.2 ± 3.1	−18.6 ± 2.8	0.6 ± 1.1

All values are mean ± SD. *MI*, Myocardial infarction; *ED*, end-diastolic phase; *ES*, end-systolic phase; *ED-ES*, distance between end-diastolic and end-systolic phases; *ALPM*, anterolateral papillary muscle; *PMPM*, posteromedial papillary muscle.

MR was achieved in the acute and chronic IMR models. More accurate, but more laborious, IMR quantification methods, such as effective regurgitant orifice area and regurgitant volume, were not used in this study. Presumably, this is only a minor limitation of this study, as the main point of interest was not IMR severity, but the exact geometric pathogenesis of tethering underlying IMR.

CONCLUSIONS

This study provides new insights into the complex interrelated and regionally heterogeneous valvular and subvalvular mechanisms involved in the geometric pathogenesis of IMR tethering. These insights result from a unique multimodal 3DE and MRI approach and may help improve future patient-tailored surgical repair techniques and results for IMR.

Conflict of Interest Statement

The authors reported no conflicts of interest.

The *Journal* policy requires editors and reviewers to disclose conflicts of interest and to decline handling or reviewing manuscripts for which they may have a conflict of interest. The editors and reviewers of this article have no conflicts of interest.

References

1. Otsuji Y, Levine RA, Takeuchi M, Sakata R, Tei C. Mechanism of ischemic mitral regurgitation. *J Cardiol*. 2008;51:145-56.
2. Timek TA, Lai DT, Bothe W, Liang D, Daughters GT, Ingels NB, et al. Geometric perturbations in multiheaded papillary tip positions associated with acute ovine ischemic mitral regurgitation. *J Thorac Cardiovasc Surg*. 2015;150:232-7.
3. Tibayan FA, Rodriguez F, Zasio MK, Bailey L, Liang D, Daughters GT, et al. Geometric distortions of the mitral valvular-ventricular complex in chronic ischemic mitral regurgitation. *Circulation*. 2003;108(Suppl 1):II116-21.
4. Beaudoin J, Dal-Bianco JP, Aikawa E, Bischoff J, Guerrero JL, Sullivan S, et al. Mitral leaflet changes following myocardial infarction: clinical evidence for maladaptive valvular remodeling. *Circ Cardiovasc Imaging*. 2017;10:e006512.
5. Gorman JH III, Jackson BM, Gorman RC, Kelley ST, Gikakis N, Edmunds LH Jr. Papillary muscle discoordination rather than increased annular area facilitates mitral regurgitation after acute posterior myocardial infarction. *Circulation*. 1997;96(9 Suppl):II124-7.
6. Gorman JH III, Gorman JH, Jackson BM, Enomoto Y, St John-Sutton MG, Edmunds LH Jr. Annuloplasty ring selection for chronic ischemic mitral regurgitation: lessons from the ovine model. *Ann Thorac Surg*. 2003;76:1556-63.
7. Gorman JH III, Gorman RC, Jackson BM, Hiramatsu Y, Gikakis N, Kelley ST, et al. Distortions of the mitral valve in acute ischemic mitral regurgitation. *Ann Thorac Surg*. 1997;64:1026-31.
8. Krawczyk- Ożóg A, Hołda MK, Bolechała F, Siudak Z, Sorysz D, Dudek D, et al. Anatomy of the mitral subvalvular apparatus. *J Thorac Cardiovasc Surg*. 2018;155:2002-10.
9. McCarthy KP, Ring L, Rana BS. Anatomy of the mitral valve: understanding the mitral valve complex in mitral regurgitation. *Eur J Echocardiogr*. 2010;11:i3-9.
10. Wijdh-den Hamer IJ, Bouma W, Lai EK, Levack MM, Shang EK, Pouch AM, et al. The value of preoperative 3-dimensional over 2-dimensional valve analysis in predicting recurrent ischemic mitral regurgitation after mitral annuloplasty. *J Thorac Cardiovasc Surg*. 2016;152:847-59.
11. Ryan LP, Jackson BM, Enomoto Y, Parish L, Plappert TJ, St John-Sutton MG, et al. Description of regional mitral annular nonplanarity in healthy human subjects: a novel methodology. *J Thorac Cardiovasc Surg*. 2007;134:644-8.
12. Levack MM, Jassar AS, Shang EK, Vergnat M, Woo J, Acker MA, et al. Three-dimensional echocardiographic analysis of mitral annular dynamics: implication for annuloplasty selection. *Circulation*. 2012;126:S183-8.
13. Kalra K, Wang Q, McIver BV, Shi W, Guyton RA, Sun W, et al. Temporal changes in interpapillary muscle dynamics as an active indicator of mitral valve and left ventricular interaction in ischemic mitral regurgitation. *J Am Coll Cardiol*. 2014;64:1867-79.
14. Miyatake K, Izumi K, Okamoto M, Kinoshita N, Asonuma H, Nakagawa H, et al. Semiquantitative grading of severity of mitral regurgitation by real-time two-dimensional Doppler flow imaging technique. *J Am Coll Cardiol*. 1986;7:82-8.
15. Bates D, Mächler M, Bolker B, Walker S. Fitting linear mixed-effects models using lme4. *J Stat Softw*. 2015;67:1-48.
16. Grewal J, Mankad S, Freeman WK, Click RL, Suri RM, Abel MD, et al. Real-time three-dimensional transesophageal echocardiography in the intraoperative assessment of mitral valve disease. *J Am Soc Echocardiogr*. 2009;22:34-41.
17. Kim K, Kaji S, An Y, Nishino T, Tani T, Kitai T, et al. Interpapillary muscle distance independently affects severity of functional mitral regurgitation in patients with systolic left ventricular dysfunction. *J Thorac Cardiovasc Surg*. 2014;148:434-40.e1.
18. Chaput M, Handschumacher MD, Guerrero JL, Holmvang G, Dal-Bianco JP, Sullivan S, et al. Mitral leaflet adaptation to ventricular remodeling: prospective changes in a model of ischemic mitral regurgitation. *Circulation*. 2009;120(11 Suppl):S99-103.
19. Nishino S, Watanabe N, Kimura T, Enriquez-Sarano M, Nakama T, Furugen M, et al. The course of ischemic mitral regurgitation in acute myocardial infarction after primary percutaneous coronary intervention: from emergency room to long-term follow-up. *Circ Cardiovasc Imaging*. 2016;9:e004841.
20. Dal-Bianco JP, Aikawa E, Bischoff J, Guerrero JL, Hjortnaes J, Beaudoin J, et al. Myocardial infarction alters adaptation of the tethered mitral valve. *J Am Coll Cardiol*. 2016;67:275-87.
21. Rausch MK, Tibayan FA, Miller DC, Kuhl E. Evidence of adaptive mitral leaflet growth. *J Mech Behav Biomed Mater*. 2012;15:208-17.
22. Langer F, Kunihara T, Hell K, Schramm R, Schmidt KI, Aicher D, et al. RING+ STRING: successful repair technique for ischemic mitral regurgitation with severe leaflet tethering. *Circulation*. 2009;120(11 Suppl):S85-91.
23. Nappi F, Lusini M, Spadaccio C, Nenna A, Covino E, Acar C, et al. Papillary muscle approximation versus restrictive annuloplasty alone for severe ischemic mitral regurgitation. *J Am Coll Cardiol*. 2016;67:2334-46.
24. Jassar AS, Minakawa M, Shuto T, Robb JD, Koomalsingh KJ, Levack MM, et al. Posterior leaflet augmentation in ischemic mitral regurgitation increases leaflet coaptation and mobility. *Ann Thorac Surg*. 2012;94:1438-45.
25. Robb JD, Minakawa M, Koomalsingh KJ, Shuto T, Jassar AS, Ratcliffe SJ, et al. Posterior leaflet augmentation improves leaflet tethering in repair of ischemic mitral regurgitation. *Eur J Cardiothorac Surg*. 2011;40:1501-7; discussion 1507.
26. Pouch AM, Wang H, Takabe M, Jackson BM, Gorman JH III, Gorman RC, et al. Fully automatic segmentation of the mitral leaflets in 3D transesophageal echocardiographic images using multi-atlas joint label fusion and deformable medial modeling. *Med Image Anal*. 2014;18:118-29.
27. Pouch AM, Aly AH, Lai EK, Yushkevich N, Stoffers RH, Gorman JH IV. Spatiotemporal segmentation and modeling of the mitral valve in real-time 3D echocardiographic images. *Med Image Comput Comput Assist Interv*. 2017;10433:746-54.
28. Puyol-Antón E, Sinclair M, Gerber B, Amzulescu MS, Langet H, De Craene M, et al. A multimodal spatiotemporal cardiac motion atlas from MR and ultrasound data. *Med Image Anal*. 2017;40:96-110.
29. Chaput M, Handschumacher MD, Tournoux F, Hua L, Guerrero JL, Vlahakes GJ, et al. Mitral leaflet adaptation to ventricular remodeling: occurrence and adequacy in patients with functional mitral regurgitation. *Circulation*. 2008;118:845-52.

Key Words: ischemic mitral regurgitation, image analysis, 3D echocardiography, magnetic resonance imaging, multimodal imaging

APPENDIX 1: EXTENDED METHODS

Surgical Protocol

Animals were treated under an experimental protocol in compliance with the National Institutes of Health's Guide for the Care and Use of Laboratory Animals (NIH publication 85-23, revised 1996) and approved by the University of Pennsylvania Institutional Animal Care and Use Committee. Healthy sheep (n = 6; mean weight, 50.2 ± 0.4 kg) were sedated with 25 to 30 mg/kg intramuscular ketamine and 0.1 mg/kg intravenous midazolam and then intubated. Anesthesia was initiated and maintained with a mixture of isoflurane (2%-5%) and oxygen throughout the procedure. Central arterial and venous access was surgically obtained in each animal.

Mitral valves and subvalvular structures were assessed at baseline with 3DE and MRI before infarction. The posterolateral infarct was induced by ligating the left circumflex artery distal to the first obtuse marginal branch for targeting an infarction of approximately 20% of the size of the LV. A prophylactic antiarrhythmic regimen of 150 mg amiodarone, 1 mg/kg lidocaine, and 1 g magnesium sulfate was administered intravenously. After 30 minutes post-MI, 3DE was performed. The animals were then monitored for several weeks, and terminal 3DE and MRI were performed at 12 weeks post-MI.

The mice were euthanized and the hearts were removed. The right ventricle and atria were excised, and the left ventricular septum was cut longitudinally from the aortic root toward the apex. The left ventricle was weighed, and an endocardial photographic image was recorded using a digital camera for determination of infarction size with planimetry software (Image Pro Plus; Media Cybernetics, Rockville, Md). The infarction area was traced manually, and infarction size was expressed in mm^2 and as percentage of LV area.

Echocardiography Protocol

The 3DE images were acquired through direct epicardial echocardiography with a Phillips ie33 ultrasound system equipped with a 2- to 7-MHz X7-2t TEE matrix transducer (Philips Medical). MR severity was determined semiquantitatively with color Doppler by assessing the area of the regurgitant jet as a percentage of left atrial area in the apical 4-chamber view. MR was graded as 0, no MR; 1, <20% MR; 2, 20% to 40% MR; 3, 40% to 60% MR; or 4, >60% MR.[29]

3DE Image Segmentation

Each full-volume 3D direct epicardial echo dataset was exported to an Echo View 5.4 workstation (TOMTEC, Unterschleissheim, Germany). Both annular and leaflet tracings were acquired at mid-systole, and annular tracings were acquired at end-systole and end-diastole. Techniques of annular segmentation and modeling and leaflet segmentation and modeling have been described previously.[9,15-17] The PMs were landmarked and confirmed with examination of the excised specimen. Once traced, measurements were derived automatically using MATLAB (MathWorks, Natick, Mass). Parameters measured are defined in Table 4.

MRI Acquisition and Reconstruction

MRI was performed with a 3-T clinical imaging system (Tim Trio, Siemens Healthcare, Erlangen, Germany) to measure LV end-systolic volume, end-diastolic volume, and muscle volume data at baseline and 12 weeks post-MI. MRI acquisition was synchronized with LV pressures. The fiber optic signal was converted to a 0 to 5 V electronic signal (O/E converter; Siemens Healthcare). The LV pressure was obtained using a pressure transducer (Mikro-Tip; Millar Instruments, Houston, Tex) and connected to a transducer amplifier (Gould, Pitman, NJ). The 0 to 5 V LV pressure and radiofrequency pulse timing were digitized at 2 kHz with a manifold analog-to-digital converter (NI USB6009 Multifunction DAQ; National Instruments, Austin, Tex), and recorded (LabView; National Instruments, Clearwater, Fla). Cine MRI data were obtained using a 2D multislice retrospectively gated cine-balanced steady-state free-precession acquisition with the following imaging parameters: echo time, 1.2 ms; repetition time, 3.9 ms; matrix, 152 × 256; field of view, 166 × 280 mm^2; flip angle, 44°; bandwidth, 930 Hz/pixel; spatial resolution, 1.1 × 1.1 mm^2; slice thickness, 4 mm. The animals received a 0.1 mmol/kg i.v. injection of gadolinium contrast for late gadolinium-enhanced cardiovascular imaging at 12 weeks post-MI.

The 2D multislice images were reconstructed with volume segmentation and processing software (Seg3D; University of Utah Scientific Computing and Imaging Institute) (Figure 1). LV mass volume was defined as the volume of the muscular structure from the ventricular apex to the MV excluding the right ventricular free wall. ALPM and PMPM volumes were defined as the volumes of the muscular structures projecting from the anterior and posterior free walls of the LV into the LV cavity, respectively. The end-diastolic volume and end-systolic volume were calculated by computing the volume of the LV blood pool at end-systole and end-diastole. Volume data were calculated with resolution of 4.84 mm^3/pixel. Linear data including left ventricular muscle thickness was also measured.

Statistical Analysis

Continuous variables were expressed as mean ± SD. Comparisons between each time point were performed by 1-way analysis of variance with Bonferroni correction. MRI data were obtained at baseline and 12 weeks post-MI, and comparisons between time points were performed using the paired-samples *t* test.

All calculations were performed using SPSS version 21.0 (IBM, Armonk, NY). Statistically significant differences were established at $P < .05$.

APPENDIX 2: ADDITIONAL RESULTS

Acute and Chronic IMR Ovine Model

Systolic pulmonary pressures and pulmonary capillary wedge pressure increased significantly relative to baseline at 30 minutes post-MI and 12 weeks post-MI, indicating acute and chronic heart failure. The average degree of MR was 0.7 ± 0.5 at baseline and was not significantly increased at 30 minutes post-MI (1.0 ± 0.6) but was seriously exacerbated to 3.2 ± 0.4 at 12 weeks post-MI (Table 5).

3DE MV Valve Annular Dilatation and Tethering Data

Epicardial 3DE showed extensive post-MI remodeling in the animal models demonstrating annular dilatation and leaflet tethering. At 12 weeks post-MI, the annular diameter and area showed marked dilation relative to both baseline and 30 minutes post-MI (Table 6). Mean MV tethering volume and MV tethering index were significantly increased, from 456 ± 206 mm^3 to 1496 ± 629 mm^3 for the former and from 0.71 ± 0.45 mm to 1.77 ± 0.52 mm for the latter. Demonstrating the restrictive leaflet movement in the systolic phase caused by IMR morphopathology, segmental tethering angles increased in most anatomic segments, with the largest increases seen in the mean P2 and P3 tethering angles, from 10.4 ± 7.5° to 27.3 ± 8.7° and from 3.3 ± 2.4° to 20.0 ± 9.0°, respectively.

Infarct Size and PM Identification

An image of the endocardial surface of the left ventricle of a resected heart 12 weeks after MI is shown in Figure 7, *A*. Mean infarct size for all animals was 22.4 ± 1.4%. The mean number of ALPM and PMPM heads identified was 2.8 ± 0.8 and 2.2 ± 0.4 per specimen, respectively (Table 7), as shown in Figure 7, *B-E*.